Asian Journal of Chemistry; Vol. 38, No. 8 (2026), 2205-2214
ASIAN JOURNAL OF CHEMISTRY
https://doi.org/10.14233/ajchem.2026.36392

Structural, Spectroscopic, Quantum Chemical and Molecular Docking Studies on 2-Aminopyridinium Dihydrogen Phosphate: A Potential Multi-Target Bioactive Molecule

G. SIVARAJ[1], N. JAYAMANI[1], T.M. VISWANATHAN[2], S. THANGARASU[3,*], S. KANNAN[4], A. MURUGAN[5,*] and B. MANIKANDAN[2]

[1]Department of Physics, Government Arts College, Salem-636007, India
[2]Department of Biotechnology, Karpagam Academy of Higher Education, Coimbatore- 641021, India
[3]Department of Physics, Kalasalingam Academy of Research and Education, Krishnankoil-626126, India
[4]Department of Physics, Government Arts College for Men, Krishnagiri-635001, India
[5]Department of Science and Humanities, Karpagam College of Engineering, Coimbatore-641032, India

*Corresponding authors: E-mail: sthangarasu@gmail.com; murugan.a@kce.ac.in

Received: 7 May 2026 *Accepted*: 29 July 2026 *Published online*: 7 August 2026 AJC-22449

Pyridine-based compounds constitute an important class of molecules with broad pharmaceutical relevance owing to their diverse biological activities. Among these, 2-aminopyridine is widely used as a versatile precursor for the construction of heterocyclic frameworks. This work describes the growth of a proton-transfer single crystal, 2-aminopyridinium dihydrogen phosphate (2APDHP), using the slow solvent evaporation technique. Single-crystal X-ray diffraction confirmed that the crystal belongs to the monoclinic system. Structural optimization was carried out at the HF and DFT levels with the 6-311++G(d,p) basis set, providing detailed information on the molecular geometry, bond distances and bond angles. The electronic characteristics were examined through frontier molecular orbital calculations. Experimental FT-IR and Raman spectra were interpreted with the aid of theoretical vibrational calculations, yielding close agreement between the calculated and observed frequencies. Molecular docking was performed to examine the interaction of 2APDHP with α-synuclein of Parkinson's disease, 6-hydroxymethyl-7,8 dihydropteroate synthase from *Mycobacterium tuberculosis* and the SARS-CoV-2 main protease.

Keywords: Infectious diseases, Molecular docking, Density functional theory, SARS-CoV-2.

INTRODUCTION

Infectious diseases remain a major cause of illness and mortality worldwide, driving the search for new therapeutic agents. Pyridine is a fundamental heterocyclic organic compound and an important structural motif in numerous pharmaceutical agents. Owing to its versatile chemical framework, pyridine and its derivatives have attracted considerable attention for their broad spectrum of biological activities and therapeutic potential against infectious diseases [1,2]. These compounds exhibit antibacterial, antifungal, antiviral, antioxidant, anticancer, anti-Parkinsonian, anti-inflammatory, analgesic and antiulcer properties [3-5]. Their strong affinity for metal ions and neutral molecules has expanded their utility to chemosensing, where they serve as efficient molecular recognition platforms for a variety of chemical species [6].

2-Aminopyridine is an important pyridine derivative widely used as a precursor for the synthesis of diverse heterocyclic compounds with significant pharmaceutical value [7,8]. Its derivatives exhibit a broad range of biological activities, including antibacterial, anticancer and anti-inflammatory effects. The increasing prevalence of antimicrobial resistance has intensified the search for new low molecular weight molecules capable of overcoming multidrug-resistant pathogens [9,10]. Owing to its simple and versatile structure, 2-aminopyridine serves as an attractive pharmacophore for the design of bioactive compounds with high synthetic efficiency and structural diversity [11-13]. Beyond antimicrobial applications, aminopyridine derivatives have therapeutic relevance in neurological disorders such as myasthenia gravis, multiple sclerosis, spinal cord injury and botulism [14]. Their broad medicinal significance has prompted extensive structural and spectroscopic investigations to better understand their physicochemical and biological properties [15].

Quantum chemical methods provide detailed insight into molecular geometry, electronic structure, vibrational characteristics and the physico-chemical properties associated with bioactive molecules [16-18]. Vibrational spectroscopy, combined with density functional theory (DFT), offers a reliable approach for understanding molecular bonding and structural features [19]. In the present study, quantum chemical calculations were performed using the Gaussian 09 package at the DFT/B3LYP level with the 6-311G(d,p) basis set. Molecular docking studies of 2-aminopyridinium dihydrogen phosphate (2APDHP) were carried out to evaluate its interactions with selected biological targets, providing computational support for its potential pharmaceutical relevance.

EXPERIMENTAL

Synthesis: Scheme-I illustrates the synthesis of 2-amino pyridinium dihydrogen phosphate single crystals. Analytical grade 2-aminopyridine and orthophosphoric acid (Sigma-Aldrich) were dissolved separately in methanol using equimolar concentrations. The solutions were mixed and stirred continuously for 4 h at room temperature to obtain a homogeneous solution. Complete dissolution was achieved by gentle heating, followed by filtration through Whatman filter paper to remove impurities. The clear filtrate was left undisturbed at ambient temperature for slow solvent evaporation. Well-defined single crystals were obtained after several days and subsequently recrystallized to improve the crystal quality and minimise structural defects.

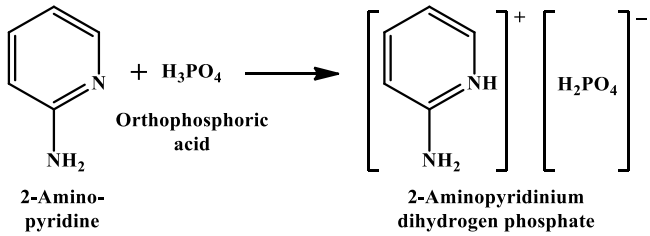

Scheme-I: Synthetic scheme of 2APDHP

Computational details: Gaussian 09W [20] programme software was used to analyses the quantum chemical computations of 2APDHP utilising HF and DFT with 6-311++G (d,p) levels [21,22]. The estimated frequencies from the experiment and the supposition were correlated. A further method for dealing with the charge exchange that takes place at molecules is HOMO-LUMO analysis. The charge transfer between the orbitals made up the charge exchange responses. The optimised molecule was visualised and the vibrational assignments were determined using Gauss View 05 [23]. The crystallographic information file (CIF) of the compound was used as an input file for the computational studies [24].

RESULTS AND DISCUSSION

Molecular geometry: Single crystal XRD analysis confirmed the grown 2APDHP ($C_5H_7N^+ \cdot 2H_2PO_4^-$) single crystals belong to monoclinic crystal system and space group $P2_1$. It has been observed that grown crystals have lattice parameters a = 9.0502 (12) Å, b = 4.5260 (3) Å and c = 9.9697 (11) Å, respectively β = 98.576 (4)º, volume V = 403.80 (7) Å^3 and Z = 2 and matched with reported data (CCDC No. 285803) [24]. Except for the unit cell parameters, the remaining information, such as bond angle, bond length and torsional angle, was taken from reported data and this CIF is used as an input file for computational studies. Moreover, the check CIF is given in the supporting information. The optimised structures of 2APDHP depicted in Fig. 1a-b are performed by HF and DFT level with 6-311++G(d,p) basis set. The optimised structural characteristics for this compound, including bond lengths, bond angles and dihedral angles, are shown in Table-1. The majority of the optimised bond lengths are a little bit larger and shorter than the experimental values, according to the theoretical values. In comparison to values obtained using the HF approach, the C-C pyridinium bond distance of the title chemical is found to have larger values using the DFT calculation [25]. The optimised bond lengths of C-C in pyridinium ring fall in the range from 1.350 Å to 1.415 Å for HF method and from 1.370 Å to 1.422 Å for DFT whereas experimental value is 1.352 Å to 1.418 Å. Fig. 1 illustrates the favourable intermolecular interaction that the hydrogen bonds have with the electronegative oxygen atoms of the PO_4^{3-} ion. Table-1 provides the geometric characteristics (bond lengths and bond angles) for the 2APDHP computed optimised structure in accordance with the atom counts in Fig. 1. The optimized geometric parameters of 2APDHP were compared with the experimental single-crystal X-ray diffraction data. As can be observed, the computed and experimental geometric parameters matched well. The N(2)-H(2A) bond length represents the biggest divergence between the estimated ground

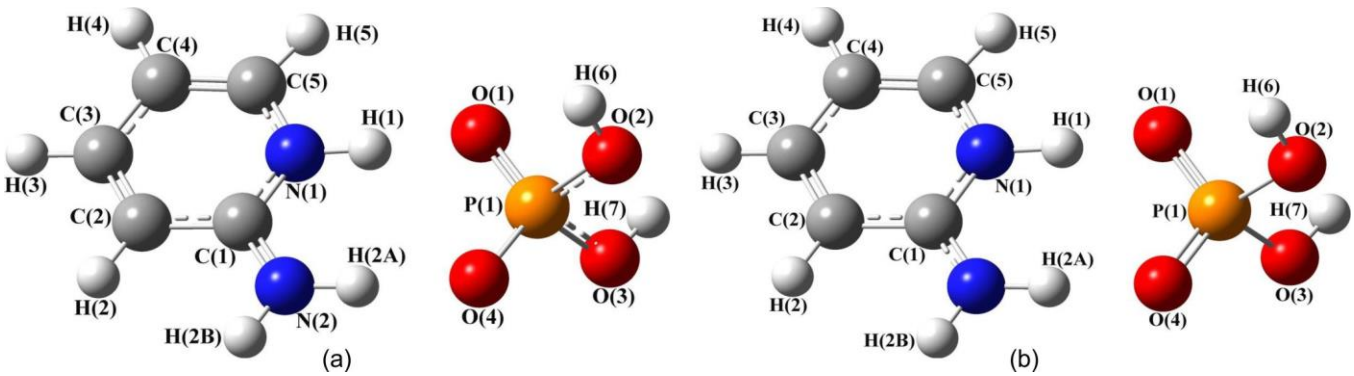

Fig. 1. Optimised molecular structure by (a) HF and (b) DFT method for 2APDHP

TABLE-1
GEOMETRICAL PARAMETERS OF 2APDHP

Bond length (Å)				Bond angle (º)			Torsional angle (º)		
Atoms connected	HF	DFT	EXP	Atoms connected	HF	DFT	Atoms connected	HF	DFT
C(1)–C(2)	1.4226	1.4224	1.418(7)	C(2)–C(1)–N(1)	117.70	117.61	N(1)–C(1)–C(2)–C(3)	0.06	0.04
C(1)–N(1)	1.3370	1.3601	1.346(6)	C(2)–C(1)–N(2)	122.68	123.28	N(1)–C(1)–C(2)–H(2)	-179.98	-179.99
C(1)–N(2)	1.3192	1.3340	1.329(6)	N(1)–C(1)–N(2)	119.62	119.11	N(2)–C(1)–C(2)–C(3)	179.93	179.85
C(2)–C(3)	1.3558	1.3726	1.367(8)	C(1)–C(2)–C(3)	119.46	119.98	N(2)–C(1)–C(2)–H(2)	-0.11	-0.18
C(2)–H(2)	1.0731	1.0828	0.9500	C(1)–C(2)–H(2)	118.82	118.73	C(2)–C(1)–N(1)–C(5)	-0.12	-0.08
C(3)–C(4)	1.4153	1.4107	1.405(8)	C(3)–C(2)–H(2)	121.72	121.28	C(2)–C(1)–N(1)–H(1)	-179.67	-179.63
C(3)–H(3)	1.0755	1.0841	0.9500	C(2)–C(3)–C(4)	121.07	120.67	N(2)–C(1)–N(1)–C(5)	-180.00	-179.90
C(4)–C(5)	1.3507	1.3703	1.352(7)	C(2)–C(3)–H(3)	119.33	119.46	N(2)–C(1)–N(1)–H(1)	0.45	0.55
C(4)–H(4)	1.0714	1.0806	0.9500	C(4)–C(3)–H(3)	119.59	119.87	C(2)–C(1)–N(2)–H(2A)	179.13	178.54
C(5)–N(1)	1.3493	1.3519	1.356(6)	C(3)–C(4)–C(5)	117.12	117.53	C(2)–C(1)–N(2)–H(2B)	1.09	1.53
C(5)–H(5)	1.0731	1.0827	0.9500	C(3)–C(4)–H(4)	121.82	121.83	N(1)–C(1)–N(2)–H(2A)	-0.99	-1.65
N(1)–H(1)	1.0507	1.1076	0.8800	C(5)–C(4)–H(4)	121.06	120.64	N(1)–C(1)–N(2)–H(2B)	-179.04	-178.66
N(2)–H(2A)	1.0243	1.0522	0.8800	C(4)–C(5)–N(1)	121.89	121.90	C(1)–C(2)–C(3)–C(4)	0.00	0.00
N(2)–H(2B)	0.9920	1.0065	0.8800	C(4)–C(5)–H(5)	123.65	123.46	C(1)–C(2)–C(3)–H(3)	179.97	179.97
P(1)–O(1)	1.4973	1.5316	1.514(3)	N(1)–C(5)–H(5)	114.46	114.64	H(2)–C(2)–C(3)–C(4)	-179.96	-179.98
P(1)–O(2)	1.6007	1.6345	1.560(4)	C(1)–N(1)–C(5)	122.75	122.31	H(2)–C(2)–C(3)–H(3)	0.01	-0.01
P(1)–O(3)	1.5885	1.6205	1.552(3)	C(1)–N(1)–H(1)	121.19	121.40	C(2)–C(3)–C(4)–C(5)	0.00	0.01
P(1)–O(4)	1.4748	1.5030	1.521(3)	C(5)–N(1)–H(1)	116.06	116.29	C(2)–C(3)–C(4)–H(4)	179.94	179.94
O(2)–H(6)	0.9415	0.9631	0.8600	O(1)–P(1)–O(2)	108.18	107.79	H(3)–C(3)–C(4)–C(5)	-179.97	-179.95
O(3)–H(7)	0.9422	0.9639	0.8000	O(1)–P(1)–O(3)	110.72	111.14	H(3)–C(3)–C(4)–H(4)	-0.03	-0.02
O(1)···H(1)	1.5607	1.4494	1.8200	O(1)–P(1)–O(4)	115.31	115.88	C(3)–C(4)–C(5)–N(1)	-0.06	-0.06
O(4)···H(2A)	1.7100	1.6378	2.0800	O(2)–P(1)–O(3)	100.06	99.38	C(3)–C(4)–C(5)–H(5)	179.90	179.89
				O(2)–P(1)–O(4)	112.47	113.07	H(4)–C(4)–C(5)–N(1)	-180.00	-179.99
				O(3)–P(1)–O(4)	109.06	108.37	H(4)–C(4)–C(5)–H(5)	-0.03	-0.04
				P(1)–O(2)–H(6)	113.58	111.66	C(4)–C(5)–N(1)–C(1)	0.12	0.10
				P(1)–O(3)–H(7)	113.92	112.38	C(4)–C(5)–N(1)–H(1)	179.70	179.67
				C(1)–N(2)–H(2A)	122.91	123.34	H(5)–C(5)–N(1)–C(1)	-179.84	-179.85
				C(1)–N(2)–H(2B)	118.65	118.34	H(5)–C(5)–N(1)–H(1)	-0.27	-0.29
				H(1)···O(1)–P(1)	117.10	117.45	C(1)–N(1)–O(1)–P(1)	5.33	7.19
				H(2A)···O(4)–P(1)	121.27	118.68	C(5)–N(1)–O(1)–P(1)	-174.24	-172.59
				H(2A)–N(2)–H(2B)	118.42	118.26	C(1)–N(2)···O(4)–P(1)	-4.64	-4.32
							H(2B)–N(2)···O(4)–P(1)	173.63	172.92
							O(2)–P(1)–O(1)···H(1)	-136.63	-139.91
							O(3)–P(1)–O(1)···H(1)	114.67	112.19
							O(4)–P(1)–O(1)···H(1)	-9.74	-12.09
							O(1)–P(1)–O(2)–H(6)	46.00	45.97
							O(3)–P(1)–O(2)–H(6)	161.88	161.87
							O(4)–P(1)–O(2)–H(6)	-82.51	-83.45
							O(1)–P(1)–O(3)–H(7)	50.26	53.26
							O(2)–P(1)–O(3)–H(7)	-63.68	-60.05
							O(4)–P(1)–O(3)–H(7)	178.15	-178.31
							O(1)–P(1)–O(4)···H(2A)	10.08	11.32
							O(2)–P(1)–O(4)···H(2A)	134.76	136.47
							O(3)–P(1)–O(4)···H(2A)	-115.18	-114.38

state geometry and the observed one (0.88). N(1)-H(1)···O(1) hydrogen bond length and angle are 1.5607/1.4494/1.820 Å and 173.56/175.42/165.0 and N(2)-H(2A)···O(4) hydrogen bond length and angle are 1.7100/1.6378/2.080 Å (HF/DFT/EXP methods respectively). Also, the dihedral angle N(1)-N(2)-O(4)-O(1) is 0.892 for HF/B3LYP calculations.

Mulliken atomic charge: Fig. 2 displays the 2APDHP atomic charge plot and Table-2 listed the estimated charge values. The fact that the carbon atom contains both positive and negative charges indicates that it is greatly influenced by its replacements [26]. The charge distribution of this molecule reveals that the hydrogen atoms have stronger electronegativity than the other carbon atoms, with H(1) = 0.7198 e/0.6315 e for HF and DFT and P(1) = 0.972 e/0.5609 e for HF and DFT, respectively. Because the phosphorus P(1) atom is surrounded by four oxygen O(1), O(2), O(3) and O(4) atoms and the hydrogen H(1) atom is surrounded by the electronegative atoms nitrogen N(1) and oxygen O(1).The hydrophilic areas are further supported by the crystal packing caused by the electronegative hydrogen H(1) atom's N-H···O interactions. The hydrogen atoms bonded to nitrogen carry positive charges due to their participation in N-H···O intermolecular hydrogen bonding.

TABLE-2
MULLIKEN CHARGE VALUES OF 2APDHP

Atom	Charge		Atom	Charge		Atom	Charge	
	HF	DFT		HF	DFT		HF	DFT
C(1)	-0.1001	-0.4177	H(2)	0.2272	0.1882	P(1)	0.9720	0.5609
C(2)	0.5116	0.6742	H(3)	0.2279	0.1794	O(1)	-0.8421	-0.6596
C(3)	-0.5120	-0.5520	H(4)	0.2285	0.1938	O(2)	-0.4944	-0.3921
C(4)	-0.3262	-0.0612	H(5)	0.2352	0.1865	O(3)	-0.4428	-0.3416
C(5)	-0.0885	-0.2435	H(1)	0.7198	0.6315	O(4)	-0.6932	-0.5178
N(1)	-0.4638	-0.2866	H(2A)	0.5382	0.4477	H(6)	0.2990	0.2808
N(2)	-0.5991	-0.4236	H(2B)	0.3112	0.2749	H(7)	0.2917	0.2778

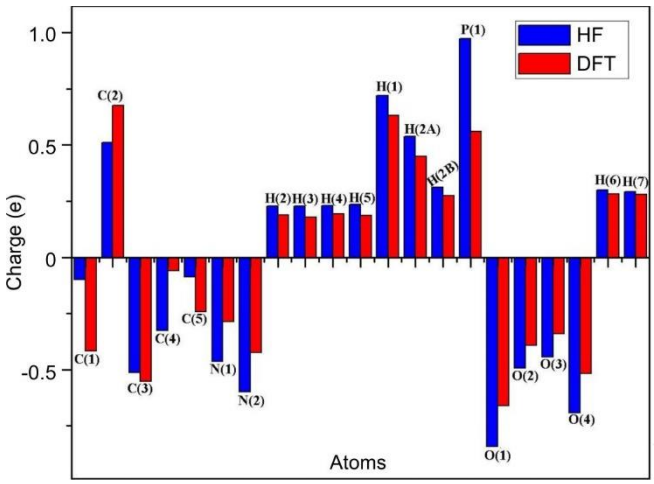

Fig. 2. Mulliken charge distributions of 2APDHP

Frontier molecular orbitals (FMO) analyses: The calculated HOMO-LUMO energy gaps of 2APDHP were 10.1475 eV at the HF level and 3.6157 eV at the DFT level (Table-3) and the corresponding orbital distributions are shown in Fig. 3. The HOMO is primarily localized over the phosphate group along the π-conjugated charge-transfer pathway, while the LUMO is predominantly distributed over the pyridinium ring, reflecting intramolecular charge transfer between these regions [27].

TABLE-3
CALCULATED MOLECULAR PROPERTIES OF 2APDHP

Molecular properties	Energy	
	HF	DFT
HOMO	-0.35058	-0.33059
LUMO	0.02193	-0.19786
$\Delta(E_{HOMO}-E_{LUMO})$ (a.u.)	0.37251	0.13273
$\Delta(E_{HOMO}-E_{LUMO})$ (eV)	10.14754	3.61570
HOMO–1	-0.4059	-0.3994
LUMO+1	0.0342	-0.1578
$\Delta E_1(E_{HOMO-1}-E_{LUMO+1})$ (a.u.)	0.44014	0.24163
$\Delta E_1(E_{HOMO-1}-E_{LUMO+1})$ (eV)	11.98985	6.58224
Ionisation potential (I)	0.35058	0.33059
Electron affinity (A)	-0.02193	0.19786
Global hardness (η)	0.18626	0.06637
Global softness (ν)	5.36898	15.06818
Electro negativity (χ)	0.16433	0.26423
Chemical potential (μ)	-0.16433	-0.26423
Global electrophilicity (ω)	0.07249	0.52599

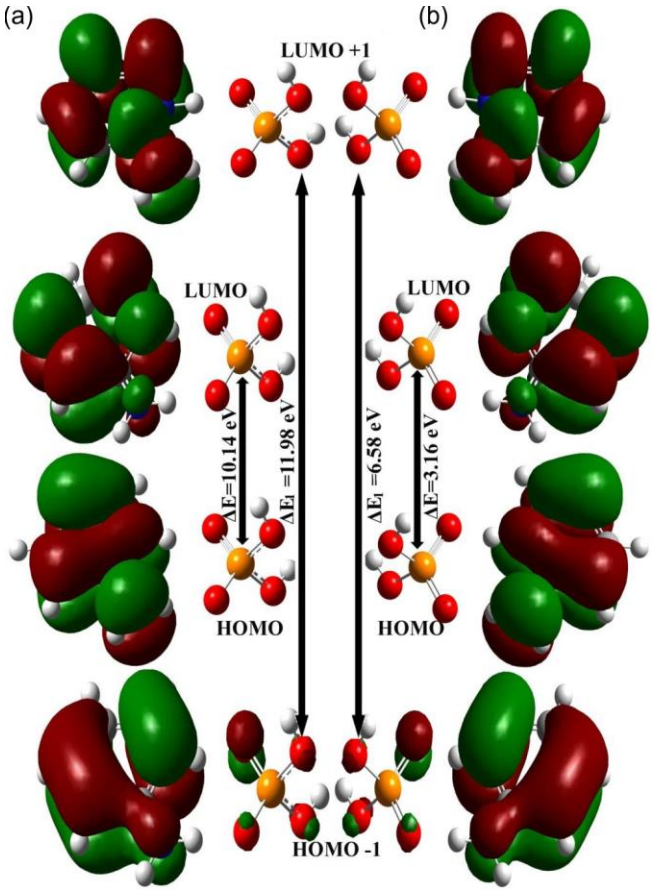

Fig. 3. FMO interaction diagram of 2APDHP (a) HF and (b) B3LYP method

Vibrational analyses: The 2APDHP molecule contains N-H, C-H, C-C, C-N, O-H and P-O functional groups. The vibrational analysis was carried out to examine the N-H···O interaction between the cation and anion, complementing the hydrogen-bonding information obtained from single-crystal X-ray diffraction. Such intermolecular interactions provide valuable insight into the structural features of the crystal. The experimental FT-IR and Raman spectra of 2APDHP are shown in Fig. 4a-b and the corresponding vibrational assignments are listed in Table-4.

N-H vibrations: The amino (NH_2) group attached to the pyridine ring exhibits six characteristic vibrational modes: symmetric and asymmetric stretching, scissoring, rocking, wagging and twisting. The stretching vibrations of primary amines generally occur in the 3500-3300 cm^{-1} region, with the asymmetric mode appearing at a higher frequency than

TABLE-4
VIBRATIONAL ASSIGNMENTS OF 2APDHP

S. No.	Frequencies		Reduced masses		Force constant		IR intensities		Raman intensities		Assignments
	HF	DFT	HF	DFT	HF	DFT	HF	DFT	HF	DFT	
1	39	34	7.1268	7.2590	0.0065	0.0048	0.1854	0.1755	2.6234	3.5400	$\gamma(CH) + \omega(NH_2)$
2	46	42	6.1401	6.0852	0.0076	0.0062	4.4004	3.8585	1.1842	1.4873	$\tau(H_2PO_3)$
3	93	94	3.7714	5.4003	0.0192	0.0283	4.5715	0.3679	0.9715	2.3767	$\gamma(CH)$
4	102	106	2.9195	5.8216	0.0180	0.0384	19.9582	5.5396	1.9337	1.4862	$\beta(CH) + \omega(NH_2)$
5	111	145	1.7136	8.5613	0.0125	0.1062	51.0060	4.3870	1.3361	0.3074	$\omega(H_2PO_4)$
6	139	151	7.8481	1.2474	0.0899	0.0168	6.8172	41.5108	0.2690	1.9586	Bending (O-H)
7	195	198	5.2743	4.1998	0.1187	0.0975	30.7263	12.5696	0.2219	0.6478	$\omega(NH_2) + \gamma(CH)$ + bending (O-H)
8	217	200	5.0738	4.2976	0.1402	0.1017	0.0212	6.7967	0.2190	0.8704	$\omega(NH_2) + \gamma(CH)$ + bending (O-H)
9	263	262	1.4303	1.6823	0.0581	0.0682	202.2348	233.3657	1.4432	0.6805	Bending (O-H)
10	402	356	4.3686	4.0475	0.4160	0.3023	19.4641	14.2479	0.3964	0.4930	Bending (O-H)
11	431	405	2.9162	2.9025	0.3195	0.2806	14.0080	14.5809	0.6880	0.5096	$\gamma(CH) + \omega(NH_2)$ + bending (O-H)
12	439	406	3.9030	3.2747	0.4436	0.3174	2.3878	6.3261	0.3432	0.7990	$\gamma(CH) + \omega(NH_2)$ + bending (O-H)
13	468	429	3.0905	1.2936	0.3995	0.1401	18.5709	42.3734	2.7827	1.7656	ω(NH of NH_2)
14	476	435	1.2230	3.1555	0.1632	0.3524	62.0242	20.9954	1.4081	3.2471	$\omega(NH_2) + \nu_{sym}$(NH) + bending (OH)
15	530	465	6.7787	7.4159	1.1211	0.9443	64.3441	60.3374	1.4001	2.1281	$\omega(PO_4)$ + bending (O-H)
16	553	500	6.9236	10.3440	1.2465	1.5244	78.1282	108.1973	0.9413	3.4994	$\omega(NH_2) + \omega(PO_4)$ + bending (O-H)
17	568	517	7.2514	6.9768	1.3790	1.0969	178.1741	132.4337	2.7579	0.7176	$\rho(NH_2) + \omega(PO_4)$ + bending (O-H)
18	573	533	2.7003	2.3830	0.5224	0.3985	95.8594	42.3390	0.8238	0.0261	$\gamma(CH) + \gamma$(NH of NH_2)
19	606	566	6.8827	6.5171	1.4876	1.2310	0.9679	15.2218	4.9794	6.3050	$\omega(NH_2) + \nu_{sym}$(N-H) + Ring vibration
20	678	636	6.1719	5.8840	1.6727	1.4021	42.3847	117.5358	5.9686	7.8750	$\beta(CH) + \nu_{sym}$(N-H) + bending (C=C)
21	804	734	2.5843	2.6760	0.9840	0.8494	7.4021	9.5248	0.1632	0.1682	$\gamma(CH)$ + bending (N-H,C-N)
22	846	772	1.5775	1.5776	0.6657	0.5544	123.8872	79.1152	0.0647	0.0393	$\gamma(CH)$
23	904	808	1.2190	11.9843	0.5866	4.6150	27.9165	126.5825	0.3582	10.9169	ν_{sym} (PO_4)
24	913	847	5.3261	1.4198	2.6156	0.5998	58.3823	0.4530	4.3730	0.3242	$\gamma(CH)$
25	918	858	6.5188	6.7997	3.2395	2.9487	40.1127	261.1417	28.9623	2.8288	ν_{asym} (PO_2) + bending (O-H)
26	938	865	1.3619	5.0573	0.7061	2.2288	1.8978	12.0830	0.7050	36.6225	$\omega(NH_2) + \beta(CH)$
27	963	906	5.8909	1.1005	3.2198	0.5322	382.2919	85.9353	1.5171	0.5291	$\gamma(CH) + \omega$(NH of NH_2)
28	1066	969	5.2372	1.3316	3.5081	0.7362	120.5552	4.2667	13.9440	0.6676	$\gamma(CH)$
29	1090	975	1.3606	3.9925	0.9533	2.2347	31.8140	442.5807	3.1025	30.9907	$\beta(CH) + \nu_{sym}$ (N-H)
30	1094	999	1.2988	1.2963	0.9164	0.7629	52.7333	0.7149	2.7326	0.2139	$\gamma(CH)$
31	1097	1010	1.3610	1.5570	0.9650	0.9357	135.0546	15.9543	1.3362	3.1021	bending (O-H)
32	1098	1015	2.1125	1.2581	1.5012	0.7636	18.5126	123.6888	1.3372	4.1035	bending (O-H)
33	1121	1049	1.3205	2.3317	0.9780	1.5118	3.8873	19.2379	0.9124	9.6500	$\beta(CH) + \rho$(NH of NH_2)
34	1165	1067	1.6230	3.5659	1.2968	2.3912	15.4352	542.7565	11.8298	16.9217	$\beta(CH)$ + bending (O-H)
35	1182	1084	7.2979	1.6449	6.0119	1.1394	717.1372	54.2883	10.4106	1.3321	$\beta(CH) + \rho(NH_2)$
36	1216	1153	1.1061	1.3593	0.9629	1.0656	108.3218	3.7670	0.5992	8.0920	$\beta(CH) + \rho(NH_2)$
37	1235	1179	1.4596	2.2969	1.3117	1.8824	5.1750	62.6687	9.8923	3.2489	$\beta(CH)$ + bending (O-H)
38	1262	1192	1.2263	1.0760	1.1506	0.9010	5.1750	63.9082	13.8509	0.9567	bending (N-H)
39	1305	1194	5.2632	1.5725	5.2825	1.3208	273.9076	124.8591	2.9309	6.5614	$\beta(CH)$
40	1356	1301	2.2495	1.7921	2.4377	1.7864	84.7411	37.3215	48.7149	17.0719	$\beta(CH)$ + bending (N-H)
41	1434	1353	1.7173	2.2250	2.0792	2.3985	57.5213	38.2311	24.5341	23.7516	$\beta(CH) + \nu_{sym}$ (C-N) + $\rho(NH_2)$
42	1507	1405	1.9120	2.2257	2.5577	2.5875	2.3399	3.4524	17.7380	13.7434	$\beta(CH)$
43	1578	1477	2.1547	2.2100	3.1603	2.8419	109.7925	50.5283	5.9025	1.6896	$\beta(CH)$ + bending (N-H)
44	1641	1533	2.2684	2.3522	3.5996	3.2552	140.8039	119.9836	7.7871	16.1761	$\beta(CH) + \omega(NH_2)$ + bending (N-H)
45	1719	1580	3.4673	3.8263	6.0392	5.6293	6.8890	7.6727	18.1445	17.0153	$\rho(NH_2) + \nu_{sym}$ (C=C) + bending (N-H)
46	1826	1672	4.4864	4.0013	8.8132	6.5938	119.1502	33.8214	8.3951	5.5051	$\beta(CH) + \rho(NH_2)$ + bending (N-H)
47	1863	1712	1.1809	1.5925	2.4148	2.7496	149.8964	245.2374	5.4004	6.0651	bending (N-H)
48	1870	1719	1.7607	1.2562	3.6277	2.1866	422.2822	163.3785	10.1084	5.2120	$\omega(NH_2)$
49	2799	2070	1.1261	1.2253	5.1962	3.0939	2248.7367	2971.2026	124.8440	73.6506	ν_{sym} (NH)
50	3286	2866	1.0844	1.0936	6.8980	5.2907	2006.6975	2676.2749	218.3875	254.5230	ν_{sym} (NH of NH_2)
51	3340	3180	1.0904	1.0884	7.1652	6.4830	2.5727	4.0659	68.3144	76.9238	ν_{asym} (CH)
52	3364	3198	1.0970	1.0948	7.3138	6.5968	2.2059	3.4714	98.2152	132.5380	ν_{sym} (CH)
53	3374	3206	1.0919	1.0906	7.3255	6.6059	0.1255	0.0407	48.1095	39.5960	ν_{asym} (CH)
54	3391	3224	1.1017	1.0981	7.4658	6.7248	0.4288	0.8085	143.2992	192.8386	ν_{sym} (CH)
55	3905	3668	1.0827	1.0798	9.7260	8.5586	100.2639	72.5176	71.0647	92.1964	ν_{sym} (NH of NH_2)
56	4179	3840	1.0662	1.0657	10.9721	9.2576	132.5546	79.0981	58.3131	104.4579	ν_{sym} (O-H)
57	4191	3854	1.0666	1.0659	11.0363	9.3267	116.7942	77.5532	54.3067	76.4658	ν_{sym} (O-H)

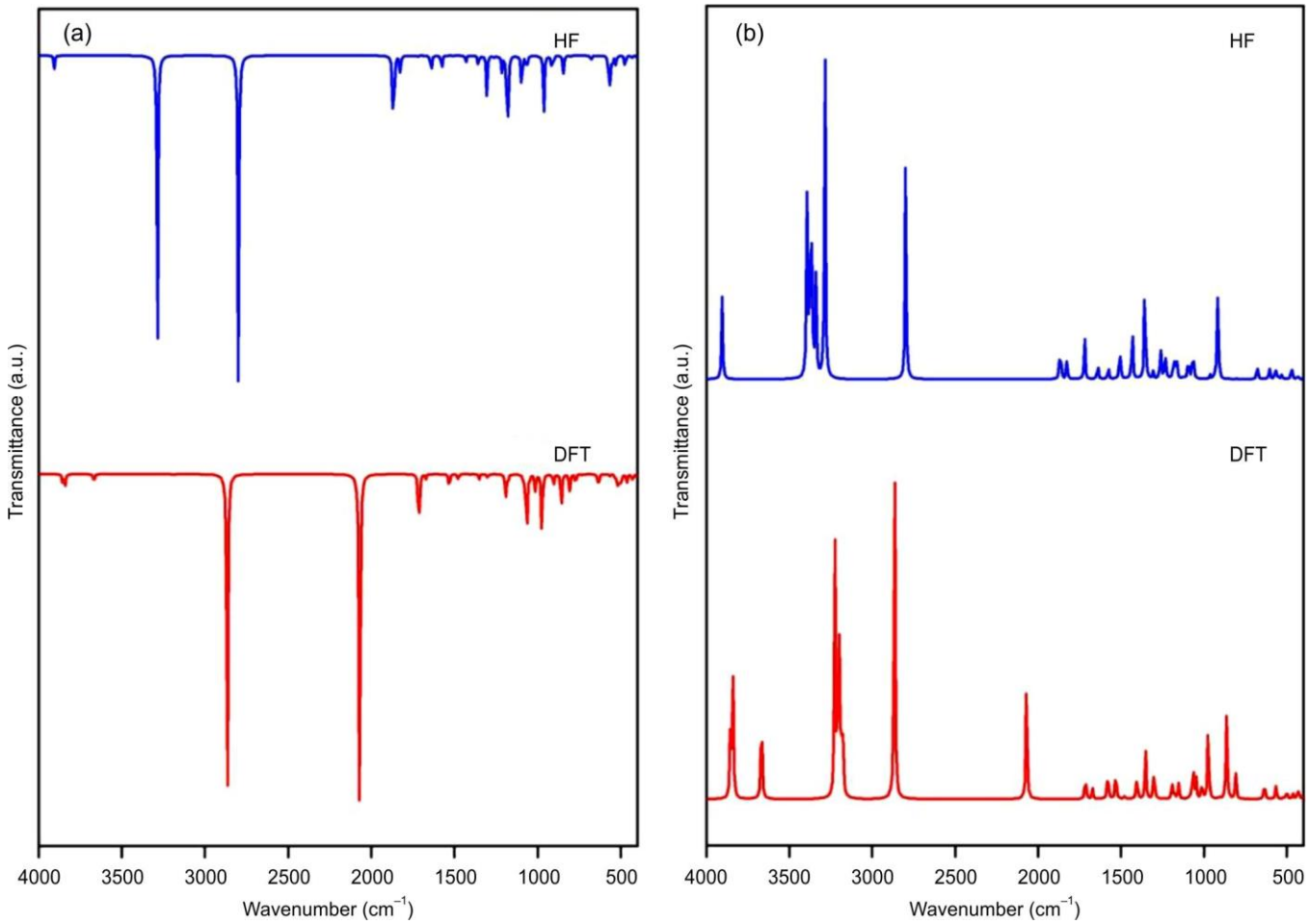

Fig. 4. Computed (a) IR spectra and (b) Raman spectra for 2APDHP

the symmetric mode [28]. In this study, the symmetric NH_2 stretching vibration was calculated at 3286 cm^{-1} (HF) and 2866 cm^{-1} (DFT). Minor differences from experimental values arise as the calculations were performed for an isolated molecule in the gas phase. The N-H···O intermolecular hydrogen bond between the dihydrogen phosphate anion and the 2-aminopyridinium cation influences the N-H stretching vibrations, resulting in a shift toward lower wavenumbers [29]. NH_2 bending vibrations were calculated at 1672 and 1580 cm^{-1} (HF), while the scissoring mode appeared at 1863 cm^{-1} (HF) and 1718 cm^{-1} (DFT) [22]. The asymmetric NH_2 stretching vibration was not observed in the calculated spectra.

C-H vibrations: The aromatic C–H stretching vibrations are generally observed in the 3100-3000 cm^{-1} region and are only slightly influenced by substituent effects [22]. In the present study, the calculated C–H stretching modes appeared at 3391 and 3364 cm^{-1} (HF) and at 3224 and 3197 cm^{-1} (DFT/B3LYP). The corresponding asymmetric stretching vibrations were obtained at 3374 and 3340 cm^{-1} (HF) and 3206 and 3180 cm^{-1} (DFT/B3LYP). The C–H bending vibration was assigned to the bands at 1090 cm^{-1} in the IR spectrum and 1121 cm^{-1} in the Raman spectrum.

C=C and C-N vibrations: The C=C stretching vibration was assigned to the band calculated at 1674 cm^{-1} using the DFT/B3LYP method. The 2APDHP molecule contains three C–N bonds, and the corresponding C–N stretching vibrations were calculated in the ranges of 1863-1578 cm^{-1} (HF) and 1353-1532 cm^{-1} (DFT/B3LYP) [21]. These vibrational modes are coupled with the in-plane bending vibrations of the C–H bonds, resulting in mixed vibrational characteristics.

H_2PO_4 vibrations: The vibrational modes of the dihydrogen phosphate anion were assigned on the basis of the calculated spectra. The P=O stretching vibration appeared as weak bands at 1182 cm^{-1} (HF) and 1067 cm^{-1} (DFT). The hydrogen bonding influences the phosphate environment, leading to a shift of the stretching frequencies toward lower wavenumbers. The P–O stretching vibrations were calculated at 882 cm^{-1} (HF) and at 963 and 857 cm^{-1} (DFT). The O–H stretching vibrations of the dihydrogen phosphate group were obtained at 4190 and 4179 cm^{-1} (HF) and at 3840 and 3854 cm^{-1} (DFT) [28].

Mechanical strength is an important factor in assessing the suitability of crystalline materials for device fabrication. Vickers microhardness testing provides valuable information on the resistance of a crystal to localized plastic deformation and assists in selecting appropriate processing conditions [28]. In present study, the Vickers microhardness of the prominent face of the 2APDHP single crystal was measured at room temperature using a microhardness tester. The Vickers hardness number (H_v) was calculated using the following relation:

$$H_v = 1.8544\frac{P}{d^2}$$

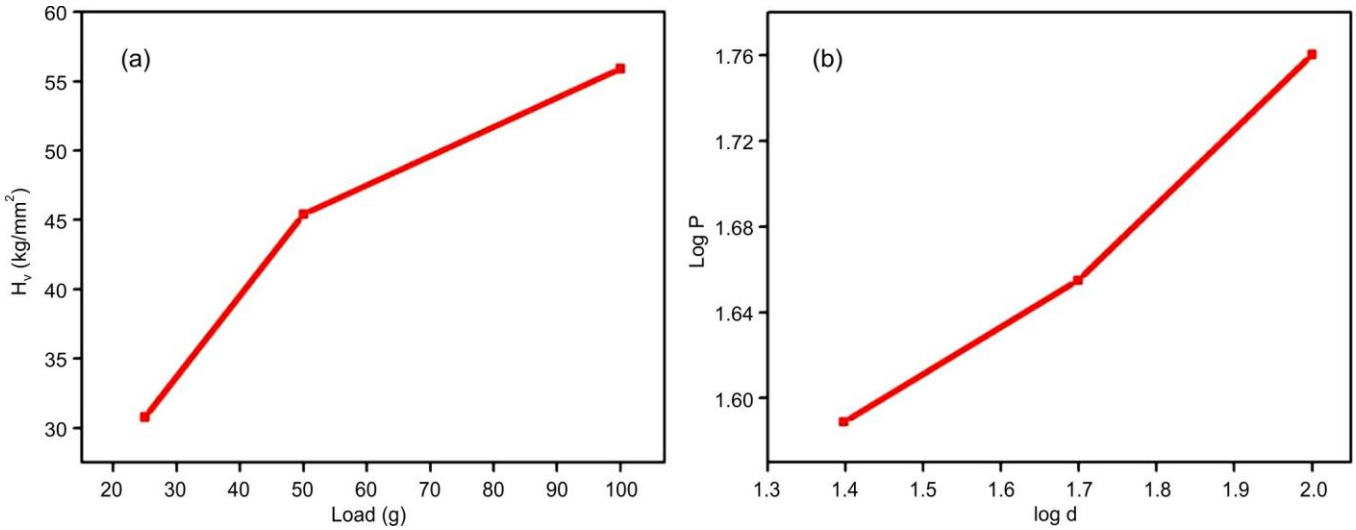

Fig. 5. (a) Plot between hardness number (H_V) and load (P); (b) variation of log P with log d

where d is the average diagonal length of the indentation (mm) and P is the applied load (g). An indentation time of 5 s was maintained throughout the measurements and the hardness values were obtained by averaging several indentations. The variation of Vickers hardness (H_V) with applied load (25-100 g) is shown in Fig. 5a. The hardness increased from 31 to 56 kg/mm^2 as the applied load increased, exhibiting a reverse indentation size effect (RISE) [30]. The Mayer index (n), determined from the slope of the log P *versus* log d plot (Fig. 5b), was 2.99. According to Onitsch's criterion, n > 2 signifies an increase in hardness with increasing load, consistent with the behaviour observed for the 2APDHP crystal [31].

The UV–Visible absorption spectrum of the 2APDHP single crystal (200-1100 nm) exhibits a sharp absorption edge at 301 nm (Fig. 6a), negligible absorption above 345 nm and high optical transparency beyond 400 nm. These optical characteristics reflect good crystalline quality with a low concentration of structural defects. The optical band gap (E_g), estimated from Tauc's plot, was found to be 3.94 eV. Such a wide band gap, together with the excellent transparency in the visible region, makes 2APDHP a suitable candidate for photonic and optoelectronic applications.

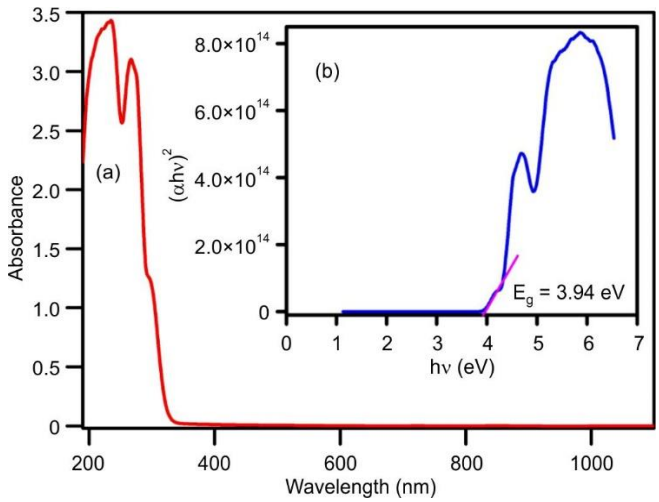

Fig. 6. (a) Optical absorbance spectrum and (b) Tauc plot for 2APDHP

Computational details: The biological potential of 2APDHP was evaluated through molecular docking against three therapeutic targets. The crystal structure of α-synuclein associated with Parkinson's disease (PDB ID: 1XQ8) [32], 6-hydroxymethyl-7,8-dihydropteroate synthase (DHPS) from *Mycobacterium tuberculosis* (PDB ID: 1EYE) [33] and the SARS-CoV-2 main protease (PDB ID: 5R7Z) [34] were retrieved from the RCSB Protein Data Bank. Active-site residues were identified from the literature and verified using CASTp [35] and the COACH metaserver [36]. Prior to docking, water molecules were removed and hydrogen atoms were added to the protein structures. A grid box covering the binding pocket was defined for each target. Molecular docking was performed using AutoDock Vina 1.2.0 after appropriate preparation of the proteins and ligand [37].

Molecular docking: The optimized structure of 2APDHP was docked against three therapeutic targets *viz*. α-synuclein (PDB ID: 1XQ8), 6-hydroxymethyl-7,8-dihydropteroate synthase (DHPS) from *Mycobacterium tuberculosis* (PDB ID: 1EYE) and the SARS-CoV-2 main protease (PDB ID: 5R7Z). The calculated binding affinities, hydrogen-bonding residues and bond distances are shown in Table-5, while the binding poses and 2D interaction maps are shown in Fig. 7.

Among the selected targets, 2APDHP exhibited the highest binding affinity toward α-synuclein (-4.3 kcal mol^{-1}), followed by DHPS (-4.1 kcal mol^{-1}) and the SARS-CoV-2 main protease (-3.8 kcal mol^{-1}). The α-synuclein complex formed three hydrogen bonds with Ser9 and Glu13 at distances of 2.3, 3.1 and 2.1 Å. A single hydrogen bond with Met130 (2.4 Å) was observed for DHPS, whereas the SARS-CoV-2 main protease formed two hydrogen bonds with Met165 and Glu166 at distances of 2.9 and 2.7 Å, respectively. The hydrophobic alkyl interactions were identified with Lys10, His131 and Met49 in the α-synuclein, DHPS and SARS-CoV-2 complexes, respectively.

The docking results support favourable interactions of 2APDHP with all three protein targets, with the strongest affinity observed for α-synuclein. These computational findings warrant further experimental validation through *in vitro* and *in vivo* studies to establish its antibacterial, antiviral and neuro-

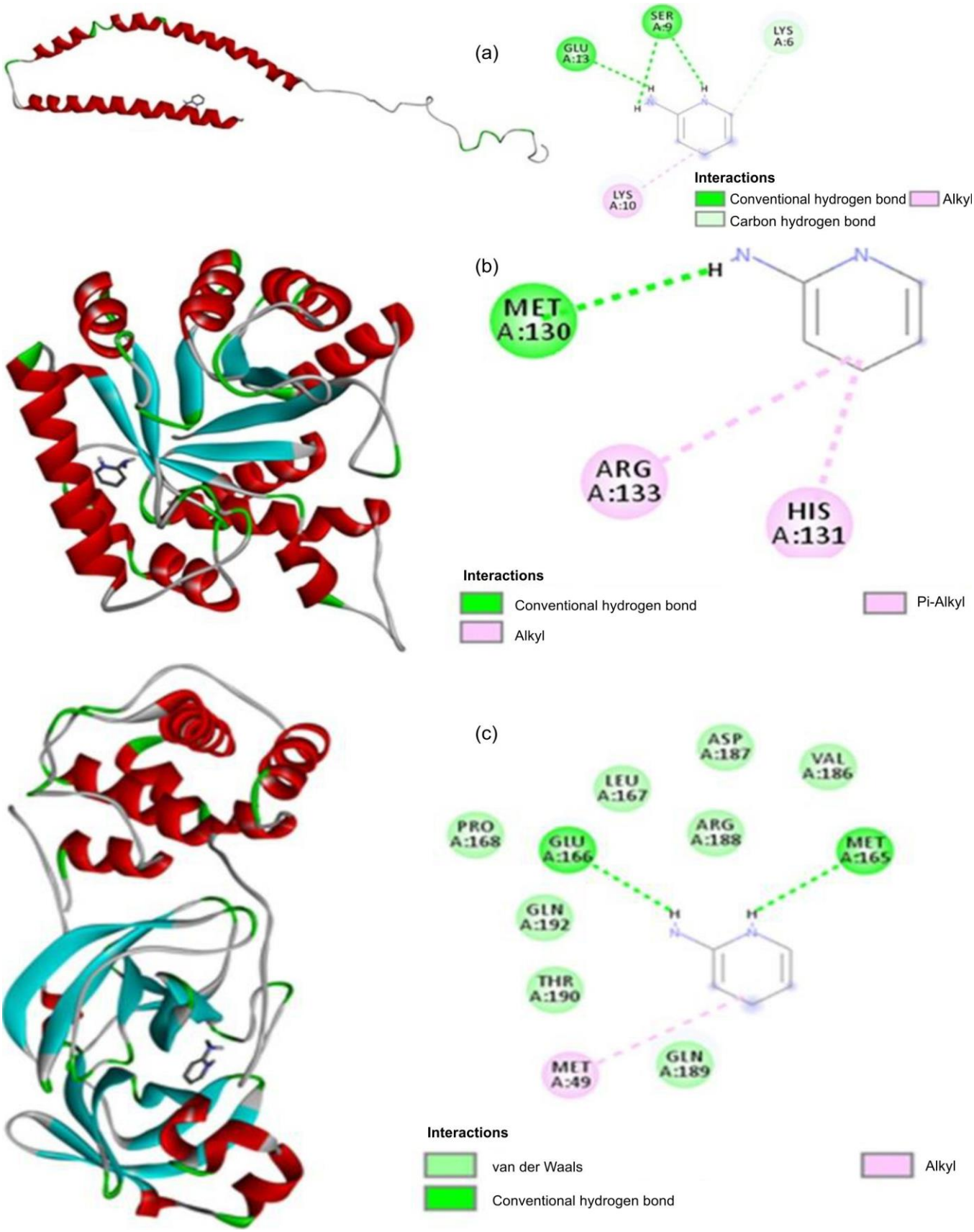

Fig. 7. Docking conformations and 2D interaction plot of 2APDHP with (a) α-synuclein of Parkinson's disease, (1XQ8), (b) 6-hydroxymethyl-7,8-dihydropteroate synthase (DHPS) of *Mycobacterium tuberculosis* (1EYE) and (c) SARS-CoV-2 virus's main protease (5R7Z) proteins

TABLE-5
BINDING AFFINITY OF 2APDHP WITH PROTEINS OF α-SYNLCEIN OF PARKINSON'S DISEASE, 6-HYDROXYMETHYL-7,8-DIHYDROPTEROATE SYNTHASE (DHPS) *M. tuberculosis* (1EYE) AND SARS-CoV-2 VIRUS'S MAIN PROTEASE (5R7Z) PROTEINS

Proteins	Binding affinity (kcal/mol)	Residues contributed for H-bonding interaction	H-bonding distance (Å)
α-Synuclein of Parkinson's disease	-4.3	Ser9 Glu13	2.3, 3.1 2.1
6-Hydroxymethyl-7,8-dihydropteroate synthase (DHPS) of *M. tuberculosis*	-4.1	Met 130	2.4
Main protease (SARS-CoV-2)	-3.8	Met 165 Glu 166	2.9 2.7

protective potential. A comparison with previous reports showed that CeO_2 nanoparticles and L-3,4-dihydroxyphenyl-alanine (L-DOPA) exhibited binding affinities of -2.1 and -3.5 kcal mol^{-1}, respectively, toward α-synuclein [38].

Conclusion

Single crystals of hydrogen-bonded 2-aminopyridinium dihydrogen phosphate (2APDHP) were successfully grown, and their structural, optical, mechanical and computational properties were investigated. The optimised geometric parameters showed good agreement with the single-crystal X-ray diffraction data, with only minor differences between the calculated and experimental bond lengths. The HOMO-LUMO energy gaps were calculated to be 10.1475 eV (HF) and 3.6157 eV (DFT), providing insight into the electronic structure of the molecule. UV-Vis analysis over the 200-1100 nm range revealed high optical transparency in the visible region and supported the presence of intramolecular charge transfer. The molecular docking studies identified favourable interactions of 2APDHP with α-synuclein, 6-hydroxymethyl-7,8-dihydropteroate synthase from *M. tuberculosis* and the SARS-CoV-2 main protease. These computational results provide a basis for further *in vitro* and *in vivo* investigations to assess the biological potential of 2APDHP.

CONFLICT OF INTEREST

The authors declare that there is no conflict of interests regarding the publication of this article.

DECLARATION OF AI-ASSISTED TECHNOLOGIES

During the preparation of this manuscript, the authors used an AI-assisted tool(s) to improve the language and no data, results or scientific conclusions were generated by AI. All analyses, interpretations and conclusions are the authors' own. The authors reviewed and edited the content and take full responsibility for the published work.

REFERENCES

1. R.E. Baker, A.S. Mahmud, I.F. Miller, M. Rajeev, F. Rasambainarivo, B.L. Rice and C.J.E. Metcalf, *Nat. Rev. Microbiol.*, **20**, 193 (2022); https://doi.org/10.1038/s41579-021-00639-z
2. D.M. Morens, G.K. Folkers and A.S. Fauci, *Nature*, **430**, 242 (2004); https://doi.org/10.1038/nature02759
3. G.M. Abu-Taweel, M.M. Ibrahim, H.M. Al-Saidi, M. Alshamrani, S. Khan, F.A. Alhumaydhi and S.S. Alharthi, *Crit. Rev. Anal. Chem.*, **54**, 599 (2024); https://doi.org/10.1080/10408347.2022.2089839
4. G.M. Abu-Taweel, S.S. Alharthi, H.M. Al-Saidi, A.O. Babalghith, M.M. Ibrahim and S. Khan, *Crit. Rev. Anal. Chem.*, **54**, 2538 (2024); https://doi.org/10.1080/10408347.2023.2186695
5. V. Siva, A. Murugan, A.S. Shameem, M.U. Priya, S. Thangarasu, S. Athimoolam and S.A. Bahadur, *J. Mol. Struct.*, **1250**, 131888 (2022); https://doi.org/10.1016/j.molstruc.2021.131866
6. M. Rajasekar, V. Ranjitha and K. Rajasekar, *Results Chem.*, **5**, 100850 (2023); https://doi.org/10.1016/j.rechem.2023.100850
7. A.C. Devi, V. Siva, S. Thangarasu, S. Athimoolam and S.A. Bahadur, *J. Mol. Struct.*, **1245**, 131033 (2021); https://doi.org/10.1016/j.molstruc.2021.131033
8. R. Mustière, A. Dassonville-Klimpt and P. Sonnet, *Future Med. Chem.*, **16**, 1357 (2024); https://doi.org/10.1080/17568919.2024.2359361
9. E.A. Fayed, A.H. Bayoumi, A.S. Saleh, E.M.E. Al-Arab and Y.A. Ammar, *Bioorg. Chem.*, **109**, 104742 (2021); https://doi.org/10.1016/j.bioorg.2021.104742
10. P. Sharma, V. Suthar, M. Aggarwal, R. Singh and K.P. Kumar, in eds.: P. Singh, Recent Developments in the Synthesis and Applications of Pyridines, Elsevier, pp. 1-42 (2023); https://doi.org/10.1016/B978-0-323-91221-1.00016-6
11. V. Siva, S.A. Bahadur, A. Shameem, S. Athimoolam, K. Udaya Lakshmi and G. Vinitha, *J. Mol. Struct.*, **1191**, 110 (2019); https://doi.org/10.1016/j.molstruc.2019.04.091
12. R.N. Rao and K. Chanda, *Chem. Commun.*, **58**, 343 (2022); https://doi.org/10.1039/D1CC04602K
13. Z. Kibou, N. Aissaoui, I. Daoud, J.A. Seijas, M.P. Vázquez-Tato, N.K. Khelil and N. Choukchou-Braham, *Molecules*, **27**, 3439 (2022); https://doi.org/10.3390/molecules27113439
14. R.A. Mekheimer, M.A. Al-Sheikh, H.Y. Medrasi and N.H.H. Alsofyani, *Molecules*, **23**, 619 (2018); https://doi.org/10.3390/molecules23030619
15. C. Carlsson, I. Rosén and E. Nilsson, *Acta Anaesthesiol. Scand.*, **27**, 87 (1983); https://doi.org/10.1111/j.1399-6576.1983.tb01911.x
16. G. Pandimeena, R. Premkumar, T. Mathavan and A.M.F. Benial, *J. Mol. Struct.*, **1231**, 129996 (2021); https://doi.org/10.1016/j.molstruc.2021.129996
17. N. Mhadhbi, S. Dgachi, A. Ben Ahmed, N. Issaoui, R. Badraoui, S. Nasr, B. Badraoui and H. Naïli, *Chem. Africa*, **6**, 1897 (2023); https://doi.org/10.1007/s42250-023-00620-8
18. U. Soykan, Y. Sert and G. Yildirim, *J. Mol. Struct.*, **1244**, 130940 (2021); https://doi.org/10.1016/j.molstruc.2021.130940
19. K. Deepakvijay, A. Prakasam, R. Arivazhagan and P.M. Anbarasan, *Chem. Phys. Impact*, **7**, 100395 (2023); https://doi.org/10.1016/j.chphi.2023.100395
20. M.J. Frisch, G.W. Trucks, H.B. Schlegel, G.E. Scuseria, M.A. Robb, J.R. Cheeseman, G. Scalmani, V. Barone, B. Mennucci, G.A. Petersson, H. Nakatsuji, M. Caricato, X. Li, H.P. Hratchian, A.F. Izmaylov, J. Bloino, G. Zheng, J.L. Sonnenberg, M. Hada, M. Ehara, K. Toyota, R. Fukuda, J. Hasegawa, M. Ishida, T. Nakajima, Y. Honda, O. Kitao, H. Nakai, T. Vreven, J.A. Montgomery, J.E. Peralta, F. Ogliaro, M. Bearpark, J.J. Heyd, E. Brothers, K.N. Kudin, V.N. Staroverov, R. Kobayashi, J.

Normand, K. Raghavachari, A. Rendell, J.C. Burant, S.S. Iyengar, J. Tomasi, M. Cossi, N. Rega, J.M. Millam, M. Klene, J.E. Knox, J.B. Cross, V. Bakken, C. Adamo, J. Jaramillo, R. Gomperts, R.E. Stratmann, O. Yazyev, A.J. Austin, R. Cammi, C. Pomelli, J.W. Ochterski, R.L. Martin, K. Morokuma, V.G. Zakrzewski, G.A. Voth, P. Salvador, J.J. Dannenberg, J. Dapprich, A.D. Daniels, Ö. Farkas, J.B. Foresman, J.V. Ortiz, J. Cioslowski and D.J. Fox, Gaussian 09, Revision E.01, Gaussian Inc., Wallingford, CT, USA (2009).

21. V. Siva, S.S. Kumar, A. Shameem, M. Raja, S. Athimoolam and S.A. Bahadur, *J. Mater. Sci. Mater. Electron.*, **28**, 12484 (2017); https://doi.org/10.1007/s10854-017-7070-8
22. V. Siva, S.S. Kumar, M. Suresh, M. Raja, S. Athimoolam and S.A. Bahadur, *J. Mol. Struct.*, **1133**, 163 (2017); https://doi.org/10.1016/j.molstruc.2016.11.088
23. R. Dennington, T. Keith and J. Millam, GaussView, Version 5, Semichem Inc., Shawnee Mission, KS, USA (2009).
24. S. Demir, V.T. Yilmaz and W.T.A. Harrison, *Acta Crystallogr. C*, **61**, o565 (2005); https://doi.org/10.1107/S0108270105024923
25. G. Sivaraj, N. Jayamani and V. Siva, *J. Mol. Struct.*, **1216**, 128242 (2020); https://doi.org/10.1016/j.molstruc.2020.128242
26. V. Siva, A. Shameem, A. Murugan, S. Thangarasu, S.A. Bahadur and S. Athimoolam, *Polycycl. Aromat. Compd.*, **43**, 4984 (2022); https://doi.org/10.1080/10406638.2022.2097711
27. A.K. Bharathi, S.C. Jeyaseelan, S. Hussain and A.M.F. Benial, *J. Mol. Struct.*, **1295**, 136551 (2024); https://doi.org/10.1016/j.molstruc.2023.136551
28. F. Dai, Q. Zhuang, G. Huang, H. Deng and X. Zhang, *ACS Omega*, **8**, 17064 (2023); https://doi.org/10.1021/acsomega.3c01336
29. G. Sivaraj, N. Jayamani and V. Siva, *J. Mol. Struct.*, **1240**, 130530 (2021); https://doi.org/10.1016/j.molstruc.2021.130530
30. V. Siva, A. Shameem, A. Murugan, S. Athimoolam, M. Suresh and S.A. Bahadur, *Chin. J. Phys.*, **64**, 103 (2020); https://doi.org/10.1016/j.cjph.2020.01.001
31. P. Vivek, G.S. Kumar, A. Steephen, R.M. Jauhar, A. Suvitha, M. Rekha, M. Kowsalya, N. Karunagaran and R. Arunkumar, *J. Mater. Sci.: Mater. Electron.*, **32**, 4493 (2021); https://doi.org/10.1007/s10854-020-05190-w
32. T.S. Ulmer, A. Bax, N.B. Cole and R.L. Nussbaum, *J. Biol. Chem.*, **280**, 9595 (2005); https://doi.org/10.1074/jbc.M411805200
33. A.M. Baca, R. Sirawaraporn, S. Turley, W. Sirawaraporn and W.G.J. Hol, *J. Mol. Biol.*, **302**, 1193 (2000); https://doi.org/10.1006/jmbi.2000.4094
34. A. Douangamath, D. Fearon, P. Gehrtz, T. Krojer, P. Lukacik, C.D. Owen, E. Resnick, C. Strain-Damerell, A. Aimon, P. Ábrányi-Balogh and J. Brandão-Neto, *Nat. Commun.*, **11**, 5047 (2020); https://doi.org/10.1038/s41467-020-18709-w
35. W. Tian, C. Chen, X. Lei, J. Zhao and J. Liang, *Nucleic Acids Res.*, **46**, W363 (2018); https://doi.org/10.1093/nar/gky473
36. J. Yang, A. Roy and Y. Zhang, *Bioinformatics*, **29**, 2588 (2013); https://doi.org/10.1093/bioinformatics/btt447
37. J. Eberhardt, D. Santos-Martins, A.F. Tillack and S. Forli, *J. Chem. Inf. Model.*, **61**, 3891 (2021); https://doi.org/10.1021/acs.jcim.1c00203
38. A.C. Kaushik, S. Bharadwaj, S. Kumar and D.Q. Wei, *Sci. Rep.*, **8**, 9169 (2018); https://doi.org/10.1038/s41598-018-27580-1